International Journal of Power Electronics and Drive System (IJPEDS)
Vol. 8, No. 3, September 2017, pp. 1147~1159
ISSN: 2088-8694, DOI: 10.11591/ijpeds.v8i3.pp1147-1159

Indirect Pulse-vector Control of Wound Rotor Induction Motor Drive in ANSYS Electromagnetics Suite

Tatiana Andreevna Funk, Yuriy Semenovich Usynin, Evgeny Viktorovich Belousov
Department of Electric Drive, South Ural State University, Chelyabinsk, Russian Federation

Article Info

Article history:

Received Jun 26, 2017
Revised Aug 5, 2017
Accepted Aug 20, 2017

Keyword:

Finite element method
Indirect control system
No motor-mounted sensor motor drive
Wound rotor induction motor pulse-vector control

ABSTRACT

This paper deals with the problem of estimation of rotor angular position for the indirect pulse-vector control of wound rotor induction motor drive. The paper considers issues of thematic justification and expanding of the field of using sensorless motor drives. With a view to improve energy consumption readings during design and modernization of motor drives of massive mechanisms with moderate standards for accuracy of velocity control, requiring long-term velocity decrease during load reduction (according to technological process conditions), using the system of the pulse-vector control of wound rotor induction motor is suggested. The paper provides the solution for the problem of developing math models of this motor drive system both for the motor-mounted sensor, and for indirect angular position sensing. The models were developed in ANSYS Electromagnetics Suite using the finite element method for studying electromagnetic processes. Based on the models, the investigation of transition and steady states of a motor drive was carried out, process quality parameters were obtained, namely: max and root-mean-square currents, torques; velocity control errors caused by pulse operation mode. From that simulation, the result illustrates the effectiveness of the proposed approach.

Corresponding Author:

Tatiana Andreevna Funk,
Department of Electric Drive,
South Ural State University,
76 Lenin prospect, Chelyabinsk, Russian Federation, 454080.
Email: kozinata@susu.ru

1. INTRODUCTION

In the recent years, indirect determination of variable coordinates of a no motor-mounted sensor motor drive, or so-called sensorless methods are coming into wider use for various mechanisms and motor drive control systems [1]-[9]. Sensorless systems enable to improve regulation characteristics of control objects with no mounting of the direct measurement device onto the motor shaft required [1],[2]. Moreover, in some cases, mounting a sensor onto the shaft can be either economically or technically unfeasible [3], or crucially impossible due to technological process conditions – for instance, because of vibration, radiation, emissions, extreme temperatures, powered motions, and isolated location of a unit from the control system.

In the general context, application of indirect methods for velocity and position determination is most relevant within the design and modernization of massive mechanism motor drives with moderate standards for accuracy of velocity control: lift-and-carry mechanisms, industrial fans, band conveyors, hydraulic pumps, compressors, air blowers, smoke and air exhausters, etc. [10].

Among them, mechanisms requiring velocity decrease during long-term load reduction or removal. For instance, fans built in industrial facilities, air exhausters in oxygen converter plants. This group may also include motor drives of band conveyors (provided that they are idle at night shifts), but in order to prevent freeze-up of bearing greasing, it is reasonable to switch them to lower rotation in no-load conditions.

In the quality of power motors in above mechanisms, induction motors with short-circuit or wound rotors are used. The motor velocity either remains non-adjustable, or is adjusted inserting ballast resistors to stator's or rotor's circuits. No adjustment or using relay-contactor circuits is accompanied by higher energy consumption. Rise in prices of electric energy and other power resources results in need for modernization of considered motor drives [6],[11].

Using two-section frequency changer in such mechanisms is not always feasible due to high cost, complicated operation, and heavy requirements for personnel qualification. There was a range of studies dedicated to the pulse-vector control (hereinafter – PVC) of wound rotor induction motor drive (hereinafter – WRIM) [12],[13]. The purpose of those systems is to create the current in the rotor with the frequency same to stators, i.e. to prevent sliding. They fairly suit the above mechanisms because of moderate cost and having no excessive adjustment capabilities, as well as show low energy consumption under low-velocity modes. Control in such system is carried out depending on the rotor angular position – thus, it is essential either to mount the position sensor onto the shaft, or to use the method for indirect rotor position determination.

Previous studies and papers on the PVC of motor drives suggested the PVC of WRIM with the rotor position sensor [12], described the developed principle and algorithm for indirect determination of the initial angular position, established differential equations and functional relationships between state variables and rotor turning angle, giving the brief explanation of the system modeling through using the finite element method [13]. The present paper sets the problem of developing an exhaustive math model and studying the PVC of WRIM, aimed at further use of the system to improve the technological process quality and enhance resource and energy consumption readings of massive mechanisms.

2. RESEARCH METHOD

2.1. The Method of the PVC of WRIM

The considered PVC [12] contains the three-phase WRIM and three-phase thyristor bridge rectifier. Shall we denote stator windings by AX, BY, CZ, and phases of three-phase powering voltage by A, B, C. The electromagnetic moment will be formed by sequential series connection of two stator phases through corresponding thyristors to two rotor windings. The magnetomotive force (hereinafter-MMF) vector of stator windings performs discrete motion with a 60-degree step. Switching is made depending on the rotor position, thereby providing the orientation of MMF vectors of stator and rotor windings to correspond to the motor torque. Either stator winding is left off the line during operation of two other ones. The tertiary rotor winding is being off the line during the whole operation cycle.

2.2. Specifics of Modeling the PVC of WRIM and Indirect Position Determination (IPD)

The considered PVC system constitutes the multi-phase, pulse, non-linear, unsymmetrical system, thus, examination of its operation in steady and transition modes by using the analytic methods for analyzing electromagnetic processes – for instance, applying differential equations of the multi-phase circuit is inclined to excessive complicating and extension of calculation conditions included as a compound of the math model. It may be reasonable to take advantage of using the progressive numerical methods for analyzing the electromagnetic system, and calculate the motor drive through using the finite element method [14].

Application of this method enables to take specifics of the motor drive system into account and significantly simplify processing and analysis of the modeling results. ANSYS Electromagnetics suite was used as it enables to: create a WRIM state space model, calculate the motor drive through using the finite element method; carry out analysis of electromagnetic processes in close relation to the powered motions and control system; analyze changes of circuit currents, electromagnetic torque, and voltages on motor windings, depending on the relative position of the stator and the rotor. In solving the problem of mathematical analysis, the experience of modeling motor drive systems using the finite element method, described in [15], was taken into account.

Modeling of the PVC system with indirect determination of the rotor angular position in ANSYS Electromagnetics Suite was divided into three stages: creating the WRIM model as a control system unit, and analysis of its operation in steady and transition modes through using the finite element method; engineering the model of the PVC system using the rotor position sensor, and analysis of motor drive operation as a control system prototype, with indirect determination of the rotor angular position; developing the model of the PVC of the induction motor with indirect determination of the rotor angular position; analysis of this motor drive system in steady and transition modes.

2.3. Architecting and Analyzing the WRIM Model

As a prototype for modeling, the crane-metallurgy wound rotor motor MTF111-6 was chosen. Nameplate data of the motor are given in Table 1.

Table 1. MTF 111-6 Motor Nameplate Data

Parameter	Unit	Value
Nominal Stator Voltage	V	380
Nameplate Angular Velocity	rpm	895
Nameplate Power	kW	3.5
Cos ϕ	-	0.73
Energy Conversion Efficiency	%	70
Nameplate Stator Current	A	10.4
Nameplate Rotor Current	A	15
Nameplate Electromotive Force on Rotor Rings	V	176
Crippling Torque	N·m	85
Pole Pairs	pcs	3

Created based on key geometric dimensions, parameters of gaps and motor windings [16], the 2D motor model is given in Figure 1(a), considering the number of pole pairs. Stator and rotor cores are made of electric steel No. 1212, induction-permeability of which was set as the non-linear property based on 24 points [17]. Motor windings are made of copper.

During architecting the model, the rotation area was created and included the rotor and motor shaft, ground potential boundaries were determined; three-phase stator and rotor windings were distributed over slots; the number of coil windings were considered; the external disturbance of windings allowing to energize winding by any electromotive force sources, was set. The grid to break the model into finite elements was selected, having higher density in the air gap and motor slots Figure 1(a), the calculation of the electromagnetic torque was set, the time step enabling to obtain correct results for shortest possible terms was determined.

Parameters obtained based on the model are as follows (values in brackets): stator (I_{1n} = 10.5 A) and rotor (I_{2n} = 15 A) currents, nameplate motor electromagnetic torque (T_n = 38 N·m), motor crippling torque (T_c = 91 N·m), nameplate sliding (s_n = 0.1), angular velocity (ω_n = 895 rpm), power coefficient (cosφ = 0.73), energy conversion efficiency (η = 0.7). All the parameters match to directory and empirical readings for this motor given in Table 1.

2.4. Modeling the PVC with Rotor Position Sensor

The principle of motor drive system operation [12] required untraditional completion of the pulse-phase control unit (PPCU) with 6 sync channels, and creation of the specific sector evaluation unit (SEU). The functional diagram of the PVC system implemented in ANSYS Electromagnetics Suite is given in Figure 1(b). Here is U_{SET} – set voltage, U_{FB} – feedback voltage proportional to circuit current, CR – current regulator, U_{CR} – current regulator output voltage, PPCU – pulse-phase control unit, U_C – set current voltage, TBR – thyristor bridge rectifier, IM – induction motor, RPS – rotor position sensor, CS – current sensor, SEU – sector evaluation unit, α_{FB} – rotor angular position.

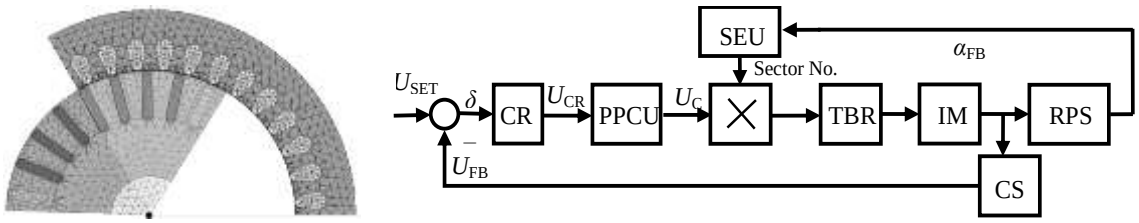

Figure 1. Segment of 2D motor model with finite element breakdown (a) and functional diagram of PPCU with rotor angular position sensor (b)

The diagram on Figure 1(b) implements the closed current control circuit. The UFB feedback waveform is compared to the USET waveform, and depending on the result of comparing δ, the PPCU forms the thyristor enabling lag waveform and U_C current set waveform. If δ reaches the maximum, the lag waveform equals zero, and enabling pulses are given to thyristors at the zero crossing of the power voltage, i.e. the whole positive half-wave of power voltage is applied to rotor windings. If δ decreases, the thyristor enabling lag increases, and the reduced positive half-wave of power voltage is applied to rotor windings.

In the considered PVC system, pulse-phase control problems differ from traditional to some extent, as according to the diagram operation principles, 6 positive half-waves of linear power voltages are

alternatively applied to motor windings: U_{AC}, U_{BC}, U_{BA}, U_{CA}, U_{CB}, U_{AB}, being out of phase against each other. The designed functional diagram of the 6-sync-channel PPCU is given in Figure 2.

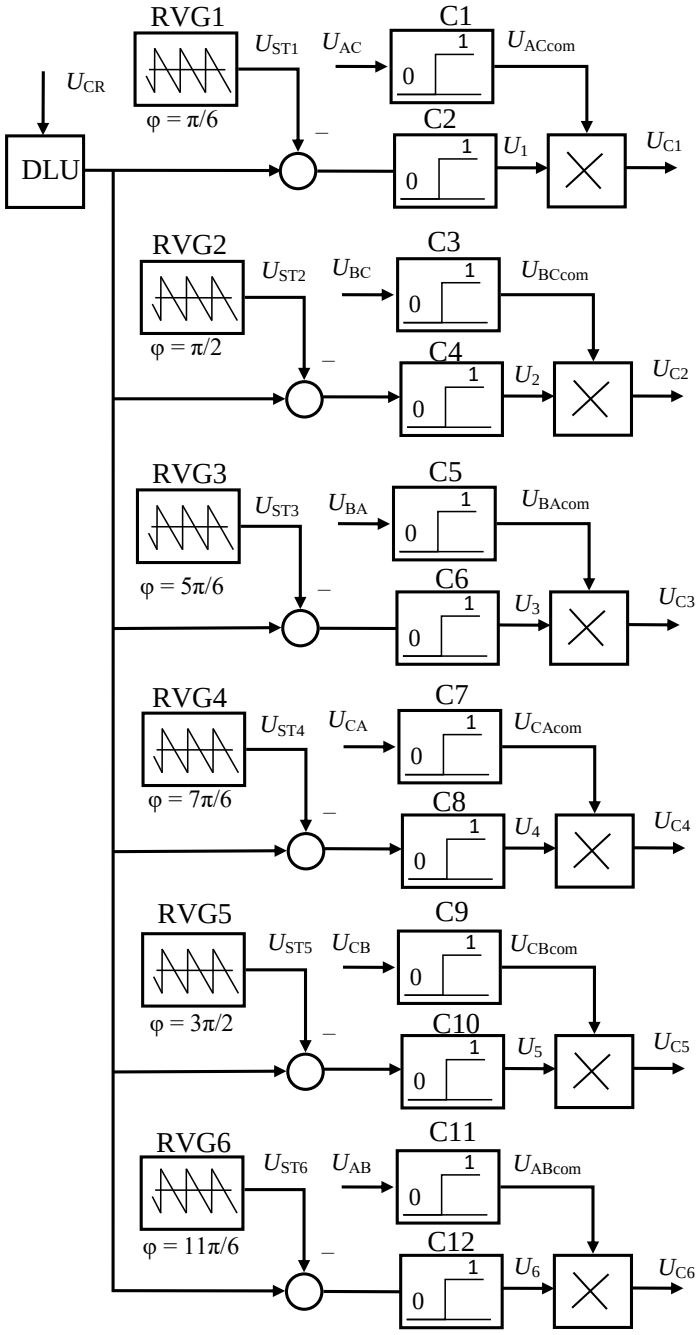

Figure 2. PPCU functional diagram

Six power voltages and current regulator (U_{CR}) output waveform are inputted to the PPCU. Output waveforms of the PPCU are six current-set waveforms: U_{C1}, U_{C2}, U_{C3}, U_{C4}, U_{C5}, U_{C6}, which, together with SEU output waveforms, form the thyristor enabling pulses. The PPCU functional diagram includes 6 comparators – corresponding to the number of sync channels. The current regulator output U_{CR} passes through the degree limitation unit DLU and is inputted to six adders. To the second input of each adder, the saw-tooth waveform is given from reference voltage generators (RVG1 – RVG6), having the phase same to that of the power voltage. Adder's output value is given to the comparator, taking a value of "1" in case of positive input waveform. In fiure 3 φ is phase shift between power voltage and reference voltage, C1 – C12

are comparators. This way, the thyristor enabling lag waveform is formed, depending on UCR current values. Figure 3(a) shows time graphs depicting the principle of the PPCU operation, through the example of the UC1 output waveform formation.

The U_{AC} power voltage is phase-shifted by $\varphi = \pi/6$. The comparator C1 acts as a syncing device, and the U_{ACcom} output waveform takes the value of "1", if the power voltage is > 0. Through using the adder, the comparison of U_{CR} and the waveform from the linearly decreasing saw-tooth voltage generator U_{ST1} (phase-shifted as the power voltage), is carried out. If $U_{CR} > U_{ST1}$, then a "1"- waveform emerges on the C2 output. U_{C1} current set waveform is formed on the product unit output (U_{ACcom} given to the first input, U_{C2} output is given to the second input).

The SEU functional diagram is showed in Figure 3(b). The waveform from the RPS is given to the SEU input, which corresponds to the rotor turning angle (in geometric degrees). The proportional unit (K = 3) transforms geometric degrees into electric degrees. The rotor turning angle (α) waveform (in electric degrees) passes through the Degree Reset Device (DRD) in case of 360-degree rotor turn. The Device includes the Sampling Unit (SU) transforming the continuous waveform α_{FB} waveform into the staircase waveform α_{SU} with sampling level 360. The adder compares α_{FB} and α_{SU}, and forms the saw-tooth waveform. For instance, if α_{FB} waveform continuously increases with time in Figure 4(a), then waveforms α_{SU} and α will look like it is showed in Figure 4(a) and (b).

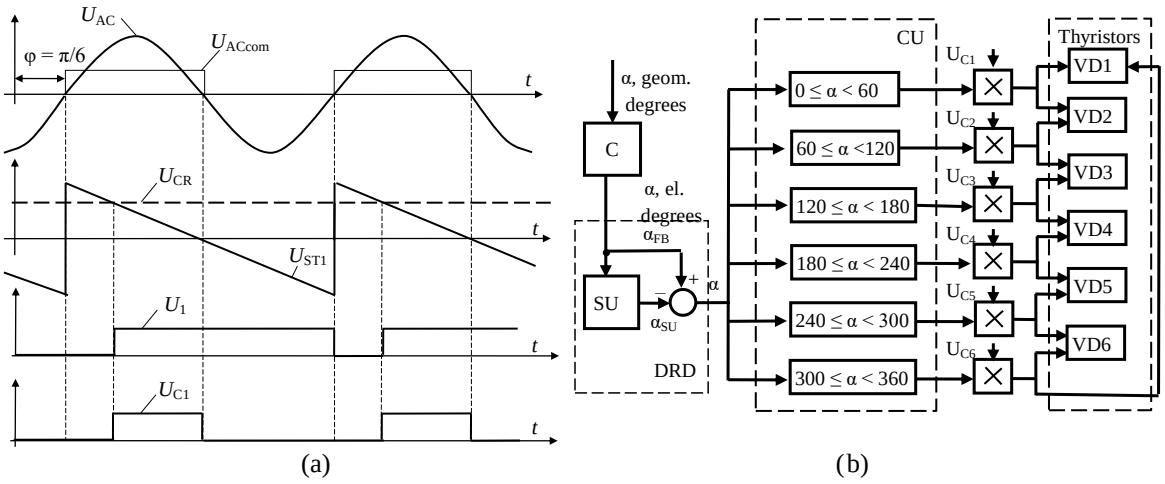

Figure 3. PPCU time graphs (a) and sector evaluation unit (SEU) functional diagram (b)

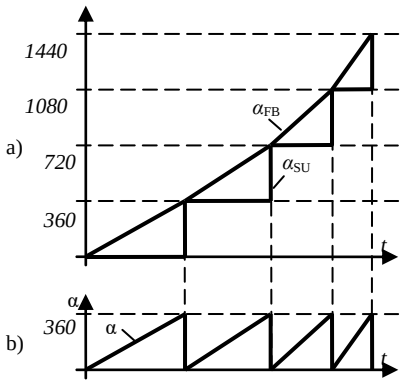

Figure 4. Degree reset device (DRD) waveforms: output SU waveform α_{SU} (a) and output DRD waveform (b)

Further, waveform α equal to the rotor turning angle (0-360 el. degrees), comes to the comparison unit (CU), where 6 conditions enable to determine the thyristor pair to set enabling pulses to. For instance, if the rotor turning angle α lies within $0 \le \alpha < 60$ electric degrees, then in case of current set waveform U_{C1}, enabling pulses are given to the first thyristor pair. A current path emerges as follows: power network

A-phase-stator winding AX-thyristor VD1-two rotor windings-thyristor VD2-stator winding BY-power network B-phase. The motor obtains the electromagnetic torque. The rotor turns clockwise. Degree α increases and reaches the value equal to or exceeding 60 electric degrees, power circuit current falls down to zero, the first thyristor pair is turned off, while enabling pulses are given to the next thyristor pair. Stator winding flux linkage vector performs a discrete motion by 60 electric degrees, etc.

By way of example, Figures 5-8 show the model-based transition processes of the pulse-vector motor drive launch with a mounted sensor. Figure 5(a) shows the dependence of the rotor turning angle α (electric degrees) on time. With such change of α, waveforms from the comparison unit, corresponding to the sector number; time graphs of thyristor currents will look like as depicted in Figures 5(b), (c).

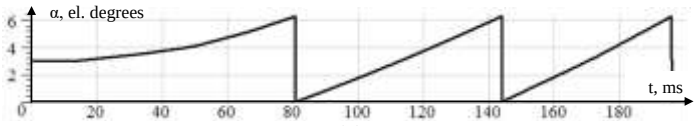

(a)

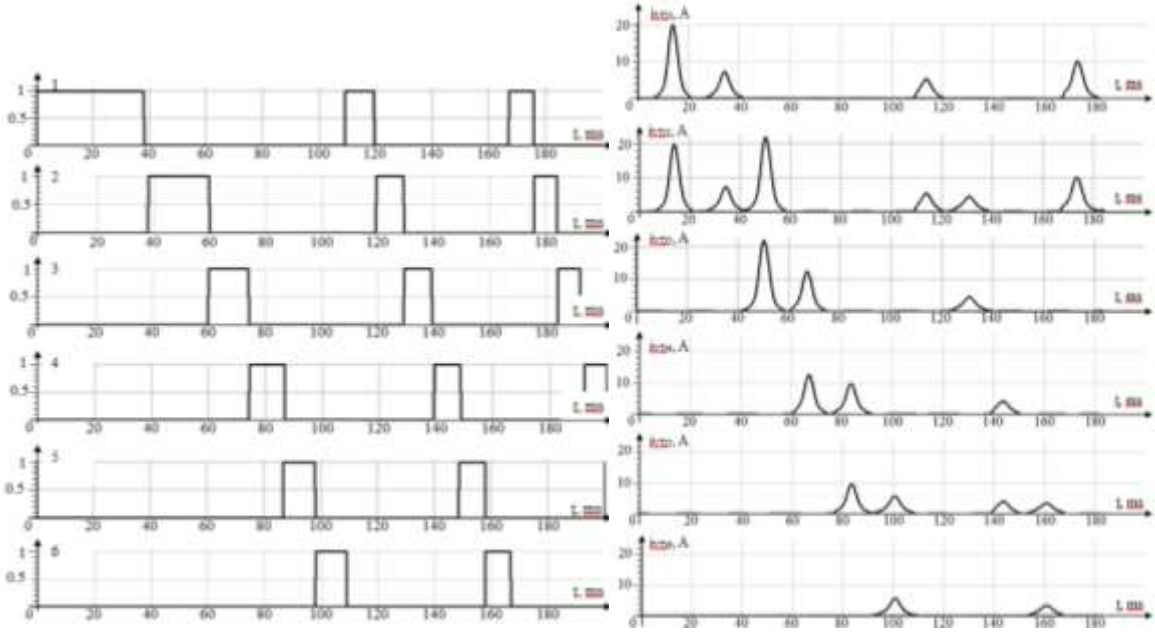

(b) (c)

Figure 5. Rotor turning angle (a), comparison unit waveforms corresponding to sector number (b) and thyristor currents time graphs (c)

At a nominal waveform in the PVC, power circuit current has the pulse nature with the max of 18 A (Figure 6). The motor obtains the electromagnetic torque as shown in Figure 7, affected by which, the motor accelerates up to 80 rad/s for 1 second as shown in Figure 8. The diagram has two types of pulse-nature, caused by thyristor commutator operation, and the torque formation principle.

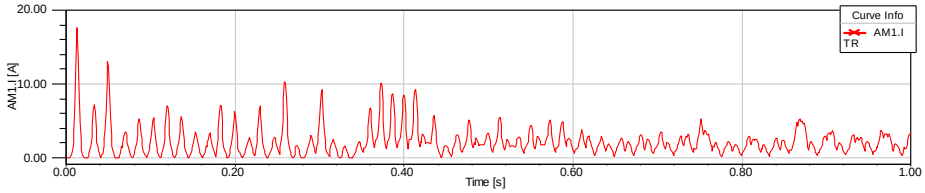

Figure 6. Transition process of power circuit current at motor start

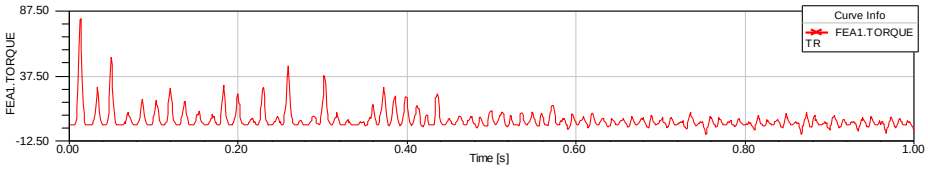

Figure 7. Transition process of motor electromagnetic torque at motor start

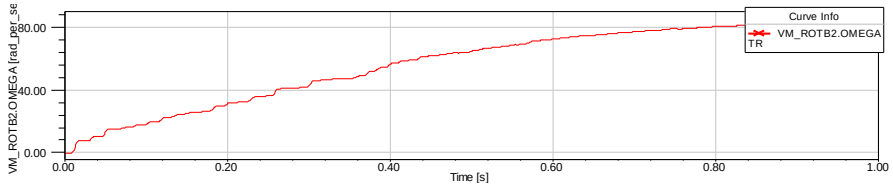

Figure 8. Transition process of motor angular velocity at motor start

2.5. Development of the PVC of WRIM with Indirect Rotor Position Determination

The indirect determination system, as well as the system with the rotor position sensor, contains the wound rotor induction motor (IM), current regulator (CR), pulse-phase control unit (PPCU), thyristor bridge rectifier (TBR), and current sensor (CS); the indirect rotor position determination unit (IRDPU) exercises the function of the rotor position sensor and sector evaluation unit as shown in Figure 9.

The IRDPU includes the initial angular position (α_0) computer (for reference on the operation procedure-see [13]), and the current angular position (α_C) computer, allowing to timely switch thyristors in transition and steady modes of the system.

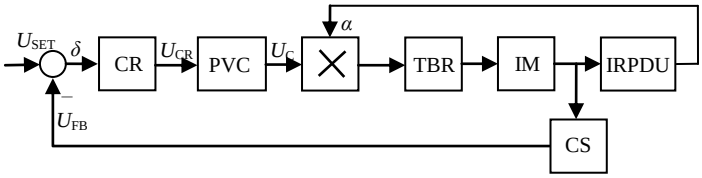

Figure 9. Functional diagram of the PVC with indirect rotor position determination

During motor operation in transition and steady modes, determination of current angular position α_C through comparing current voltages on motor winding (as it was done to determine α_0), does not seem possible. Calculation of α_C based on instantaneous voltages is also difficult due to presence of points having ambiguous values – for instance, zero crossing points. That is why indirect calculation of α_C was performed based on root-mean-square rotor winding voltages, in 3 steps. For convenient operation, stator windings voltages U_{AX}, U_{BY}, U_{CZ} were used as accessible for direct measurement of electric parameters within indirect calculation of α_C.

The indirect α_C computer includes three voltage sensors (VS) measuring stator windings voltages - VS_{AX}, VS_{BY}, VS_{CZ}, and root-mean-square voltages units – RMS_{AX}, RMS_{BY}, RMS_{CZ}. The functional diagram of the IRPDU (α_C) is given in Figure 10. To the input of the unit, instant voltages on stator windings – u_{AX}, u_{BY}, u_{CZ} – are given; thyristor control waveforms are the output. The IRPDU contains 6 sector determination channels, by the number of sectors. Channels alternatively form the thyristor control pulses in case if the corresponding condition is met when comparing voltages on stator windings.

Let us consider the principle of IRPDU (α_C) operation through the example of the first sector determination channel (Channel 1). The Channel 1 Functional Diagram within Interaction with other Channels is given in Figure 11. During operation, thyristors VD2 and VD5 are enabled in the first sector, and the current goes through stator windings AX and CZ, while stator winding BY remains unenergized.

Maximum positive motor electromagnetic torque is reached at $U_{CZ} > U_{AX}$. It is essential to feed enabling pulses to thyristors VD2 and VD5 when $U_{CZ} > U_{AX}$ condition is met. Verification of meeting the condition goes as follows. Root-mean-square voltages U_{CZ} and U_{AX} come to the adder $S1_1$ (the subscript indicates a channel an element belongs to); if the adder output waveform $\delta 1 > 0$, then on the output of the

voltage comparing unit V_{CU1}, the waveform U_{VCU1} is formed, bearing the "1"-value; if $\delta 1 < 0$, then $U_{VCU1} = 0$.

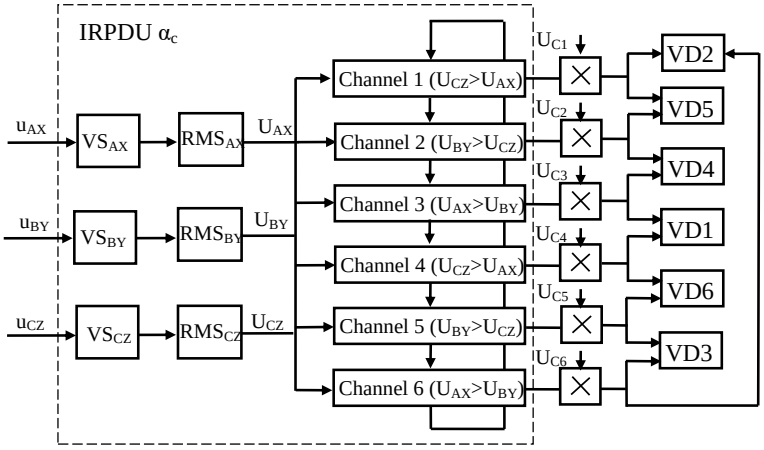

Figure 10. IRDPU α_c Functional Diagram

The waveform U_{VCU1} is fed to the first waveform-inverting comparator $IC1_1$. The waveform U_{VCU1} is fed to the first waveform-inverting comparator $IC1_1$. Then, from the comparator, the waveform comes to the integrator I_1 with the time constant T = 0.001 and single saturation zone. Thus, as long as the integrator input waveform equals zero, the waveform $U_{I1} = 0$ is formed on the integrator output, which is fed to the second inverting comparator $IC2_1$, forming the "1"-value on the output. If at this very moment, there is a waveform from the previous-channel comparator, which reports on finishing operation and it is time for enabling the next thyristor pair, thyristors VD2 and VD5 receive enabling pulses. Once U_{CZ} becomes lower than U_{AX}, $\delta 1 \leq 0$, and U_{VCU1} equals zero, then the integrator input (after the inverting comparator $IC1_1$), receives the "1"-value, output integrator waveform reaches the "1"-value for t = 0.001 s, $IC2_1$ acts, and enabling pulse feeding to thyristors VD2 and VD5 is halted. On the output of the third inverting comparator $IC3_1$, the waveform permitting enabling second-sector thyristors is formed.

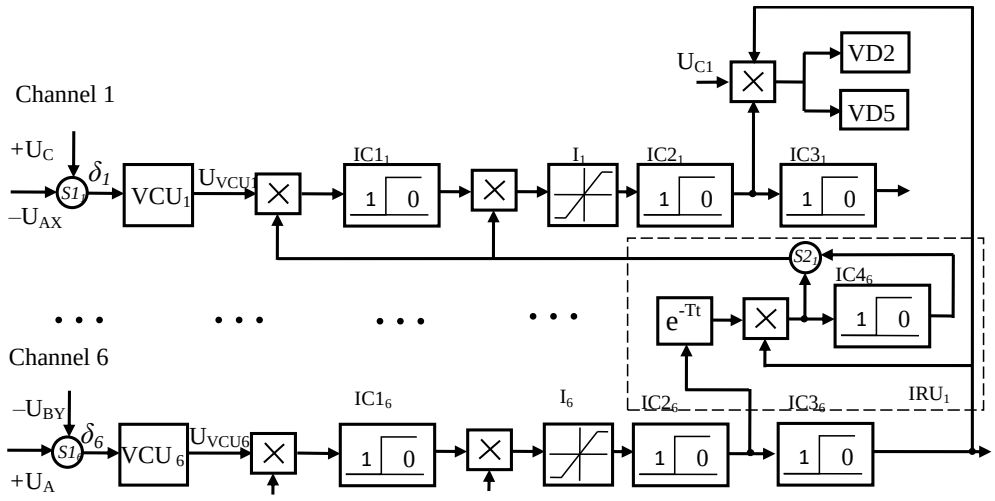

Figure 11. Channel 1 functional diagram within interaction with other channels

The integrator I_1 will not leave the saturation zone until it receives the "-1"-value waveform on the input. The reset waveform will come to the integrator after the rotor comes all 6 sectors and turns 360 degrees. Then, all the processes repeat. This pulse is formed by the integrator reset unit IRU_1, which contains

the pure delay element, product element, inverting comparator $IC4_1$, and adder $S2_1$. Presence of integrators with the saturated zone in the IRPDU provides protection from false acts. Other sector determination channels operate the similar way.

By way of example, Figures 12-15 show the transition processes of the no-load launch of the PVC with the indirect determination of rotor angular position. Figure 12 depicts the dependence of the rotor turning angle α (electric radians) from time (t = 800 ms). At such change of α, IRPDU-originated waveforms corresponding to the sector number, and time graphs of thyristor currents, will look like as showed in Figures 13, 14.

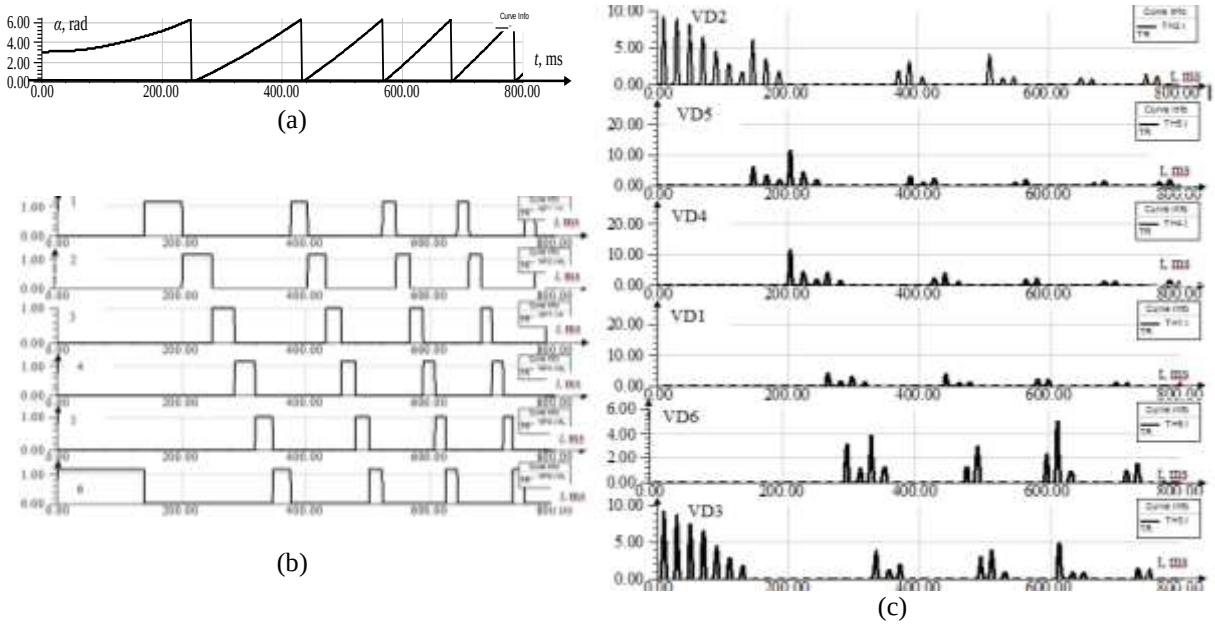

Figure 12. Rotor turning angle (radians) (a), IRPDU waveforms corresponding to sector number (b) and thyristor currents time graphs (c)

In case of half-waveform in the PVC, power circuit current has the pulse nature with the maximum of 10 A as shown in Figure 13. The motor obtains the electromagnetic torque as shown in Figure14, affected by which, the motor accelerates up to 20 rad/s for 0.8 seconds as shown in Figure 15.

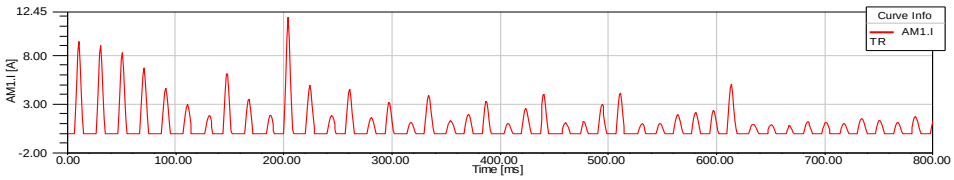

Figure 13. Power circuit current at motor start

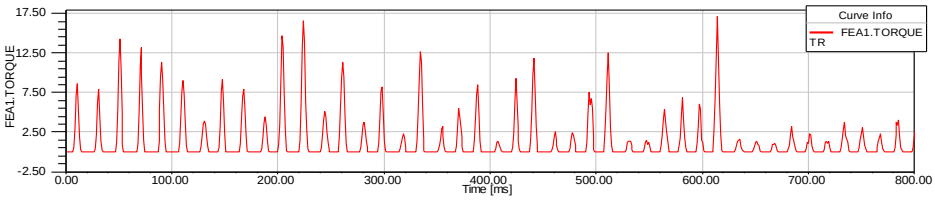

Figure 14. Motor electromagnetic torque at motor start

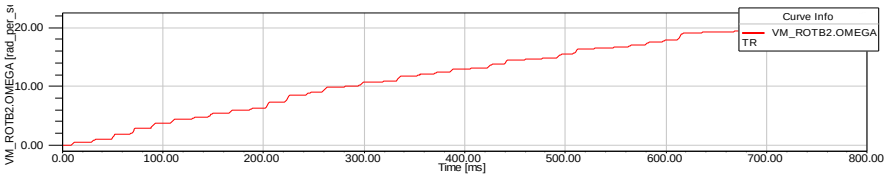

Figure 15. Motor angular velocity at motor start

Figure 16 depicts the fragment of forming thyristor-enabling pulses based on 3-step-averaged voltages (U_{AX}, U_{BY}, U_{CZ}). Within the time range t_1-t_2, $U_{AX} \geq U_{BY}$, on the output of the Channel 6, the "1"-value is formed, enabling pulses are fed to thyristors VD3 and VD2. At t_2, voltage U_{AX} becomes lower than U_{BY}, the waveform U_6 disappears, Channel 1 starts operating. Within the time range t_2-t_3, the condition $U_{CZ} \geq U_{AX}$ is met, and the waveform $U_1 = 1$ is formed on the Channel 1 output, while enabling impulses are fed to thyristors VD2 and VD5.

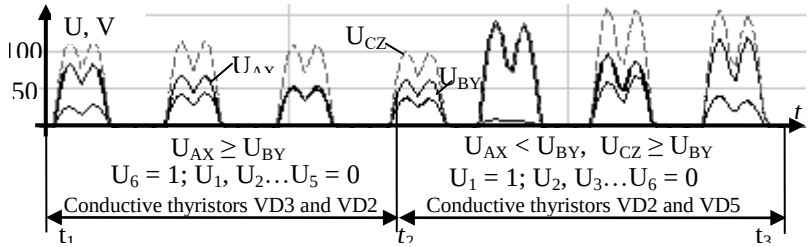

Figure 16. Fragment of Forming Enabling Pulses Based on Averaged Voltages

3. RESULTS AND ANALYSIS

3.1. Process Quality Paramters for the PVC of WRIM with Rotor Position Sensor and with Indirect Rotor Angular Position Determination

Mechanisms that the PVC is positioned to, require ensuring auxiliary low-velocity low-static-torque modes. That is why it makes sense to analyze process quality parameters obtained on the ANSYS-based math model, for low angular velocities. In this context, let us consider the following process quality parameters: the ratio of maximum and root-mean-square power circuit currents of the nameplate stator current I_{max}/I_{1N} and I_{RMS}/I_{1N}; the ratio of maximum and average motor electromagnetic torques of the nameplate torque T_{max}/T_N and T_{AV}/T_N; the ration of velocity fluctuation of the nameplate synchronous velocity $\Delta\omega/\omega_{0N}$, caused by the pulse-nature operation mode. Control process quality parameters obtained in ANSYS Electromagnetics Suite for the PVC of WRIM bouth with rotor position sensor and with indirect rotor angular position determination, are given in aggregate in Table 2. for absolute and relative values. For explanation, Figure 17 depicts the determination of quality parameters for the 0.2 ratio between the angular velocity and the nameplate synchronous velocity ω_{0N}.

Table 2. Process Quality Parameters

Parameter	for the PVC of WRIM with RPS						for the PVC of WRIM with RPD					
T_{AV}/T_N	0	0.1	0.2	0.3	0.4	0.5	0	0.1	0.2	0.3	0.4	0.5
T_{AV}, N·m	0	3.7	7.4	11.1	14.8	18.5	0.0	3.7	7.4	11.1	14.8	18.5
T_{max}/T_N	0.2	0.6	1.8	2.8	3.2	4.1	0.2	0.3	0.7	1.8	3.0	3.3
T_{max}, N·m	8.6	23.5	65.7	102.0	118.0	150.0	9.2	9.8	24.9	68.2	110	123
I_{RMS}/I_{1N}	0.2	0.3	0.3	0.5	0.6	0.8	0.2	0.2	0.3	0.3	0.5	0.6
I_{RMS}, A	2.5	2.7	3.6	5.0	6.2	8.0	2.4	2.5	2.7	3.6	5	6.2
I_{max}/I_{1N}	0.4	0.6	1.3	1.8	2.2	3.3	0.4	0.6	1.3	1.7	2.2	2.5
I_{max}, A	4.1	6.3	14.0	18.5	22.5	33.9	4.2	6.2	13.8	18.1	23	26
ω_{av}/ω_{0N}	0.9	0.8	0.5	0.3	0.2	0.1	0.9	0.8	0.5	0.3	0.2	0.2
ω_{av}, rad/s	96.4	85.0	50.0	26.8	21.0	9.6	98	88	52	29	25	20
$\Delta\omega/\omega_{0N}$	0.02	0.03	0.04	0.07	0.11	0.11	0.02	0.03	0.04	0.07	0.11	0.12

At a glance, current and torque ratios $I_{max}/I_{1N} < T_{max}/T_N$ and $I_{RMS}/I_{1N} < T_{AV}/T_N$, may prompt questions, as in most cases the current grows faster than the torque, but in the considered diagram, stator and rotor windings form the series circuit – here emerges the effect typical for series-excitation motors, when the differential torque runs ahead the differential current.

3.2. Comparing indirect determination and rotor position sensor systems

Examination of the PVC of WRIM in ANSYS Electromagnetics Suite figured their efficiency when used as control systems of massive mechanism motor drives with moderate standards for accuracy of velocity control, requiring velocity decrease during long-term load reduction or removal. Based on quality parameters considered in Paragraph 3.1, comparison of the model of motor drive with indirect determination rotor angular position determination and the pulse-vector control with rotor position sensor, revealed the indirect-determination system shows fair results as well. The rotor angular position computer implemented in ANSYS Electromagnetics Suite, possesses the relatively plain structure and requires 3 voltage sensors on stator windings to measure the current rotor position, and the programmed controller possessing minor computing powers as compared with famous methods for indirect determination of the state vector [2]. With that, position computer provides for correct rotor angular position determination accurate within a sector, meeting the necessary and sufficient criterion of successful PVC operation. In cases when rotor position determination accuracy must be enhanced, further voltage analysis of the stator unenergized winding can be carried out.

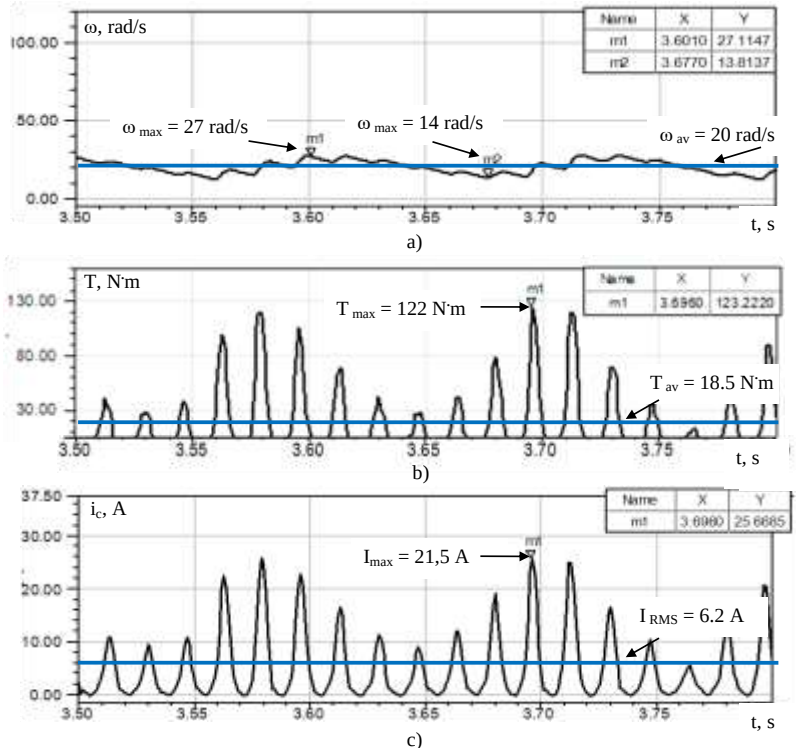

Figure 17. Fragment of ANSYS calculation curves of motor drive velocity control mode: a) velocity ω; b) electromagnetic torque T; c) circuit current i_c

4. CONCLUSION

The models of the pulse-vector control of wound rotor induction motor drive with the rotor position sensor and indirect position determination were developed by means of ANSYS Electromagnetics Suite. Implementation of the untraditional pulse-phase control unit syncing thyristor-enabling pulses with the network in the pulse-vector control system, ensured meeting required motor torque values in the half-wave detection circuit.

Examinations carried out in ANSYS Electromagnetics Suite figures that the method of indirect rotor angular position is appropriate. The pulse-vector control with indirect rotor angular position determination is operable, having quality parameters being highly competitive with those of the sensor-mounted system.

Properties of the PVC with indirect determination and process quality parameters enable to infer that the problems stated in the introduction were successfully solved.

Application of the developed PVC with indirect determination will allow carrying out modernization of massive mechanisms with moderate standards for accuracy of velocity control, velocity decrease during load reduction or removal, with as low economic costs as possible – both during modernization itself, and during further operation.

ACKNOWLEDGEMENTS

The work was supported by Act 211 Government of the Russian Federation, contract № 02.A03.21.0011

REFERENCES

[1] I. M. Alsofyani and N. R. N. Idris, "A Review on Sensorless Techniques for Sustainable Reliablity and Efficient Variable Frequency Drives of Induction Motors," *Renewable and Sustainable Energy Reviews*, vol. 24, pp. 111-121, 2013.
[2] J. Holtz, "Sensorless Control of Induction Motor Drives," *Proceedings of the IEEE*, vol/issue: 90(8), pp. 1359–1394, 2002.
[3] J. C. Gamazo-Real, *et al.*, "Position and Speed Control of Brushless DC Motors Using Sensorless Techniques and Application Trends," *Sensors*, vol/issue: 10(7), pp. 6901-6947, 2010.
[4] C. M. Verrelli, *et al.*, "Nonlinear Tracking Control for Sensorless Permanent Magnet Synchronous Motors with Uncertainties," *Control Engineering Practice*, vol. 60, pp. 157-170, 2017.
[5] Z. Qiao, *et al.*, "New Sliding-mode Observer for Position Sensorless Control of Permanent-magnet Synchronous Motor," *IEEE Transactions on Industrial Electronics*, vol/issue: 60(2), pp. 710-719, 2013.
[6] D. A. Dominic and T. R. Chelliah, "Analysis of Field-oriented Controlled Induction Motor Drives under Sensor Faults and an Overview of Sensorless Schemes," *ISA Transactions*, vol/issue: 53(5), pp. 1680-1694, 2015.
[7] M. H. Holakooie, *et al*., "Full-order Luenberger Observer Based on Fuzzy-logic Control for Sensorless Field-oriented Control of a Single-sided Linear Induction Motor," *ISA Transactions*, vol. 60, pp. 96-108, 2016.
[8] M. Beschi, *et al*., "Sensorless Model-based Object-detection Applied on an Underactuated Adaptive Hand Enabling an Impedance Behavior," *Robotics and Computer-Integrated Manufacturing*, vol. 46, pp. 38-47, 2017.
[9] S. Derammelaere, *et. al.*, "Sensorless load angle control for two-phase hybrid stepper motors," *Mechatronics*, vol. 43, pp. 6-17, 2017.
[10] M. Montanari, *et. al.*, "Speed Sensorless Control of Induction Motors Based on a Reduced-Order Adaptive Observer," *IEEE Transactions on Control Systems Technology*, vol/issue: 15(6), pp. 1049-1064, 2007.
[11] P. Shinde, *et al.*, "Speed Control of Induction Motor by Using Variable Frequency Drive," *Rupali Burungale et al Int. Journal of Engineering Research and Applications*, vol/issue: 4(4), pp. 35-37, 2014.
[12] Y. S. Usynin, *et al.*, "Asynchronous Electric Drive with Pulse-vector Control," *Russian Electrical Engineering*, vol/issue: 82(3), pp. 134-137, 2011.
[13] Y. S. Usynin, *et al.*, "Pulse-vector Control with Indirect Determination of Rotor Angular Position," *Russian electrical engineering*, vol/issue: 84(10), pp. 566-571, 2013.
[14] M. A. Iqbal and V. Agarwal, "Investigation & Analysis of Three Phase Induction Motor Using Finite Element Method for Power Quality Improvement," *International Journal of Electronic and Electrical Engineering*, vol/issue: 7(9), pp. 901-908, 2014.
[15] Y. S. Usynin, *et al.*, "Synthesis of Control System by Electrical Drive with Synchronous Reluctance Independent Excitation Machine," *Bulletin of South Ural State University. Series: Power Engineering*, vol/issue: 18(37), pp. 38-41, 2012.
[16] Y. V. Alekseev, *et al.*, "Crane Electrical Equipment: Reference Book," Moscow, Energiya Publishing House, pp. 240, 1979.
[17] I. P. Kopylov, "Handbook of electrical machines: 2 tons," Moscow, Energoatomizdat Publishing House, pp. 688, 1989.

BIOGRAPHIES OF AUTHORS

Tatiana Andreevna Funk received the PhD degree from South Ural State University, Chelyabinsk, Russian Federation, in 2012. She is currently an Associate Professor in the Department of Electric Drive, South Ural State University, Chelyabinsk, Russian Federation. Her research interests include motor drive control systems with motor-mounted sensor and indirect control systems.

Yuriy Semenovich Usynin received the PhD degree from Moscow Power Engineering Institute, Moscow, Russian Federation in 1994. He is currently a Professor in the Department of Electric Drive, South Ural State University, Chelyabinsk, Russian Federation. His research interests include motor drive control systems and the electric drive with the field regulated reluctance machine.

Evreniy Viktorovich Belousov received the PhD degree from South Ural State University, Chelyabinsk, Russian Federation, in 2014. He is currently an Associate Professor in the Department of Electric Drive, South Ural State University, Chelyabinsk, Russian Federation. His research interests include the electric drive with the field regulated reluctance machine and electric transport.